УДК 539.612

NANOPARTICLE ADHESION AND FLOW PROPERTIES OF COHESIVE NANOPOWDERS

Jürgen Tomas

Mechanical Process Engineering,
The Otto-von-Guericke-University Magdeburg, Germany

Represented by a member of the Editorial Board Professor E. Tsotsas

Key Words and Phrases: adhesion forces; cohesion; constitutive models; particle mechanics; powder mechanics; powder compressibility; powder flow properties; titania nanopowder; van der Waals forces.

Abstract: The fundamentals of cohesive powder consolidation and flow behaviour using a reasonable combination of particle and continuum mechanics are explained. By means of the model "stiff particles with soft contacts" the influence of elastic-plastic repulsion in particle contacts is demonstrated. With this as the physical basis, the stationary yield locus, instantaneous yield loci and consolidation loci, flow function, consolidation and compression functions by the flow properties of a very cohesive titania nanopowder (surface diameter d_s = 200 nm) are presented. These models are used to evaluate shear cell test results as constitutive functions for computer aided design of process apparatuses for reliable powder flow.

Symbols

a – separation, nm
A – area, particle contact area, m²
C_H – Hamaker constant, J
d – particle size, μm
E – modulus of elasticity, kN/mm²
F – force, N
p – pressure, kPa
p_f – plastic yield strength of particle contact, MPa
r – radius, nm
ε – porosity
κ – elastic-plastic contact consolidation coefficient
κ_A – elastic-plastic contact area coefficient
κ_p – plastic contact repulsion coefficient
φ – angle of friction, deg
ρ – density, kg/m³
σ – normal stress, kPa
σ_1 – major principal stress, kPa
σ_0 – isostatic tensile strength, kPa
τ – shear stress, kPa

Indices

b – bulk
c – compressive
K – total contact
e –effective
el – elastic
H – adhesion
i – internal
l – liquid
M –centre of Mohr circle
N – normal
pl – plastic
R – radius of Mohr circle
s – solid
sls – solid-liquid-solid
st – stationary
VdW – van der Waals
Z – tensile
0 – initial, zero point.

Introduction

The well-known flow problems of cohesive particulate solids in storage and transportation containers, conveyors or process apparatuses - mainly mentioned by Jenike [1] – leads to bridging, channelling, oscillating mass flow rates and particle characteristics

associated with feeding and dosing problems. Taking into account this list of selected technical problems and hazards, it is worth to deal with the fundamentals of particulate solids consolidation and flow, i.e., to develop a reasonable combination of particle and continuum mechanics. This method appears to be appropriate to derive constitutive functions on physical basis in the context of micro-macro transition of particle-powder behaviour.

Particle Contact Constitutive Model

The well-known failure hypotheses of Tresca, Coulomb-Mohr, Drucker and Prager, the yield locus concept of Jenike [1] and Schwedes [2, 3] were supplemented from Molerus [4, 5] by the cohesive steady-state flow criterion. The consolidation and non-rapid, frictional flow of fine and cohesive particulate solids was explained by the adhesion forces at particle contacts [4]. His advanced theory is the suitable basis of the extended model approach [27 to 30] which is shown now.

In principle, there are four essential mechanical deformation effects in particle-surface contacts and their force-response behaviour can be explained as follows:

(1) *elastic* contact deformation (Hertz [6], Huber [7], Mindlin [8], Dahneke [9], Derjaguin (DMT theory) [10], Johnson (JKR theory) [11], Thornton [12] and Sadd [13]) which is reversible, independent of deformation rate and consolidation time effects and valid for all particulate solids;

(2) *plastic* contact deformation with adhesion (Derjaguin [14], Krupp [15], Schubert [16], Molerus [4, 5], Maugis [17], Walton [18] and Thornton [19]) which is irreversible, deformation rate and consolidation time independent, e.g. mineral powders;

(3) *viscoelastic* contact deformation (Yang [20], Rumpf [21] and Sadd [13]) which is reversible and dependent on deformation rate and consolidation time, e.g. soft particles as bio-cells;

(4) *viscoplastic* contact deformation (Rumpf [21]) which is irreversible and dependent on deformation rate and consolidation time, e.g. nanoparticles fusion.

These force-displacement models are shown as characteristic constitutive functions in Fig. 1. Based on these theories, a general approach for the time and deformation rate dependent and combined viscoelastic, elastic-plastic, viscoplastic, adhesion and dissipative behaviours of a spherical particle contact was derived [28,29] and is briefly explained here - the comprehensive review of Tomas [41] comprises all the derivations in detail:

During approaching of the spheres, the adhesion force F_{H0} without any additional contact deformation, see Fig. 2, *a*), can be modelled as a single rough sphere-sphere-contact, additionally, with a characteristic hemispherical micro-roughness height or radius $h_r < d$ instead of particle size d [25, 26]:

$$F_{H0} = \frac{C_{H,sls} h_r}{12 a_{F=0}^2} \left[1 + \frac{d / h_r}{2\left(1 + h_r / a_{F=0}\right)^2} \right] \approx \frac{C_{H,sls} h_r}{12 a_{F=0}^2}. \qquad (1)$$

If an external compressive normal force F_N is acting at a *soft* contact of two isotropic, *stiff*, linear elastic, mono-disperse spherical particles the previous contact point is deformed to a small contact area, Fig. 2, and the adhesion force between these two particles is increasing, Krupp [15], Rumpf et al. [21] and Molerus [4, 5]. After this loading and elastic deformation, Fig. 2, *b*), the contact starts at $p_{max} = p_f$ with plastic yielding. This elastic-plastic contact deformation response in Fig. 2, *c*) is given by the particle

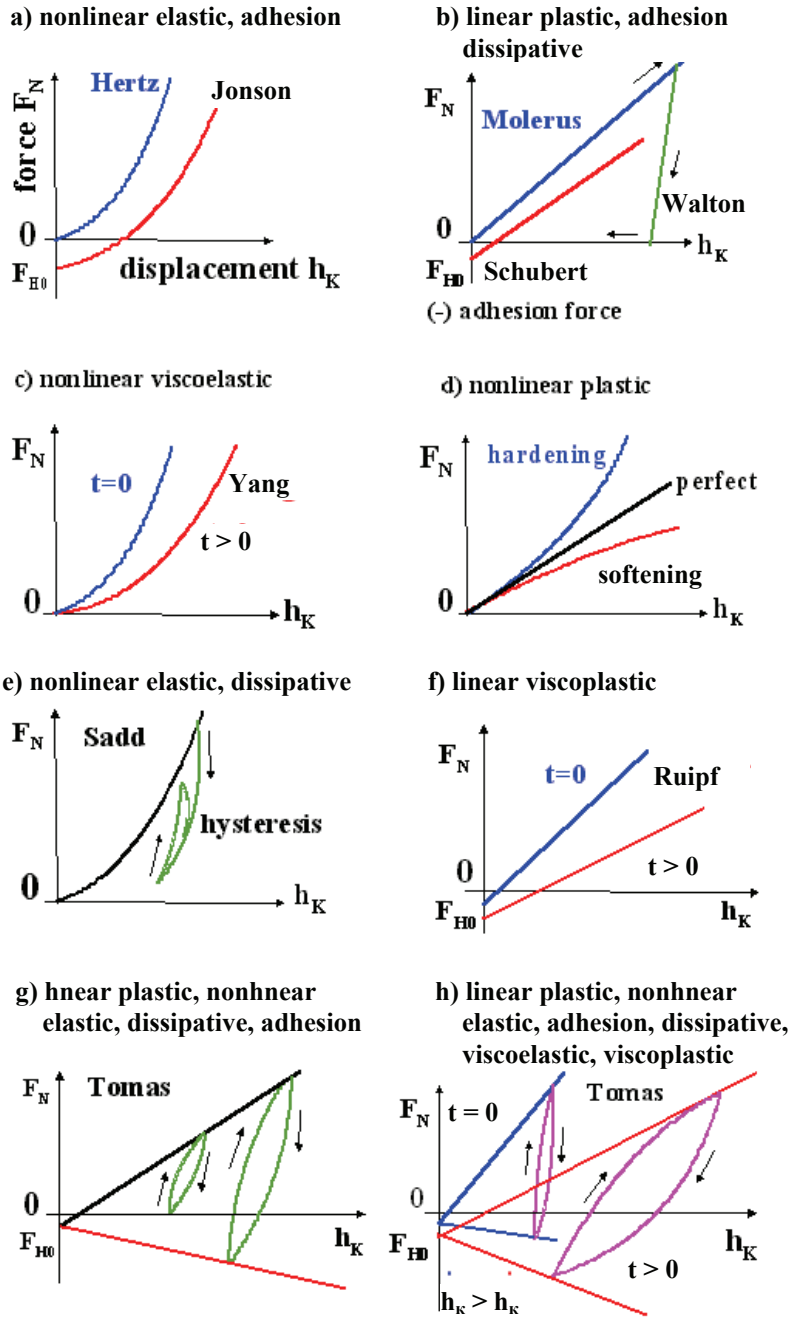

Fig. 1 Force – displacement diagram of constitutive models of contact deformation of smooth spherical particles in normal direction without/with adhesion (compression +, tension -). *The basic models for elastic behaviour were derived by Hertz* [6], *for viscoelasticity by Yang* [20], *for constant adhesion by Johnson et al.* [11] *and for plastic behaviour by Thornton and Ning* [19] *and Walton and Braun* [18] *and for plasticity with variation in adhesion by Molerus* [4] *and Schubert et al.* [16]. *This has been expanded stepwise to include nonlinear plastic contact hardening and softening. Energy dissipation was considered by Sadd et al.* [13] *and time dependent viscoplasticity by Rumpf et al.* [21]. *Considering all these theories, one obtains a general contact model for time and rate dependent viscoelastic, elastic-plastic, viscoplastic, adhesion and dissipative behaviours, Tomas* [28, 29]

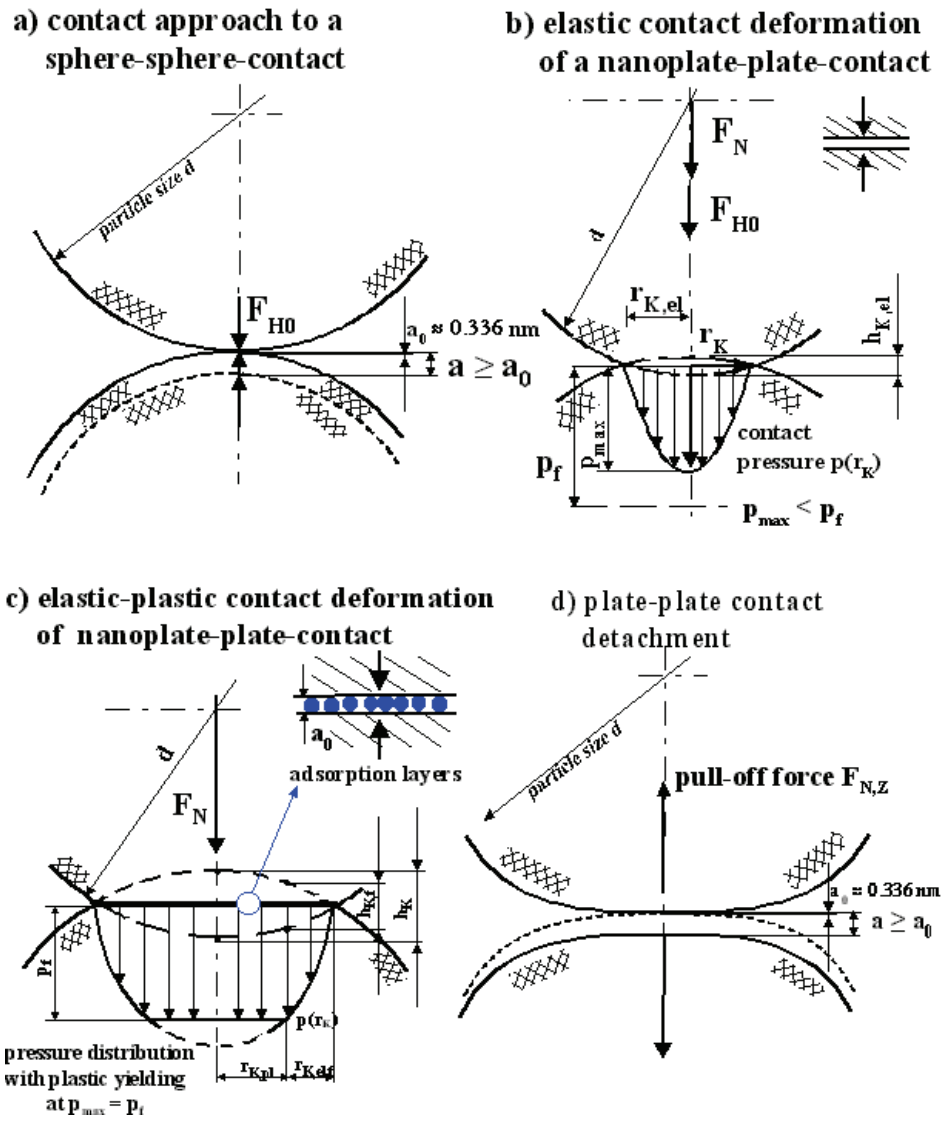

Fig. 2 Particle contact approach, elastic, elastic-plastic deformation and detachment. *After loading with an external force F_N the spherical contact is elastically compacted to a plate-plate-contact and shows the Hertz* [6] *elliptic pressure distribution b). With increasing normal load this contact starts at the yield point $p_{max} = p_f$ with plastic yielding c). The micro-yield surface is reached and this maximum pressure has not been exceeded. A hindered plastic field is formed at the contact with a circular constant pressure p_{max} and an annular elastic pressure distribution dependent on radius $r_{K,el}$, full lines in c)*

contact force equilibrium between attraction (–) and elastic as well as *soft* plastic repulsion (+) or force response (r_K^* coordinate of annular elastic contact area):

$$\sum F = 0 = -F_{H0} - p_{VdW}\pi r_K^2 - F_N + p_f \pi r_{K,pl}^2 + 2\pi \int_{r_{K,pl}}^{r_K} p_{el}(r_K^*) r_K^* dr_K^* . \qquad (2)$$

Superposition provided, this leads to a very useful linear force displacement model (for $\kappa_A \approx$ const) with the particle centre approach of both particles h_K [28], shown in Fig. 3 as elastic-plastic boundary (averaged radius of particle *1* and *2* $r_{1,2} = \left(1/r_1 + 1/r_2\right)^{-1}$):

$$F_N + F_{H0} = \pi r_{1,2} p_f \left(\kappa_A - \kappa_p\right) h_K . \tag{3}$$

Thus, the contact stiffness decreases with smaller size $d = 4r_{1,2}$ (or micro-roughness radius) of cohesive powders and nanoparticles, predominant plastic yielding behaviour provided [28]:

$$k_{N,pl} = \frac{dF_N}{dh_K} = \pi r_{1,2} p_f \left(\kappa_A - \kappa_p\right) . \tag{4}$$

The plastic repulsion coefficient κ_p describes a dimensionless ratio of attractive Van der Waals pressure p_{VdW} to repulsive particle micro-hardness p_f for a plate-plate model:

$$\kappa_p = \frac{p_{VdW}}{p_f} = \frac{C_{H,sls}}{6\pi a_{F=0}^3 p_f} \tag{5}$$

The characteristic adhesion distance in Eqs. (1) and (5) lies in a molecular scale $a = a_{F=0} \approx 0{,}3\ldots0{,}4$ nm. It depends mainly on the properties of liquid-equivalent packed adsorbed layers and can be estimated for a molecular interaction potential minimum $-dU/da = F = 0 = F_{at} + F_{rep}$ or force equilibrium. It depends mainly on the properties of liquid-equivalent packed adsorbed layers and can be estimated for a molecular interaction potential minimum $-dU/da = F = 0 = F_{at} + F_{rep}$ or force equilibrium [22]. Provided that these molecular contacts are stiff enough compared with the soft particle contact behaviour, this separation $a_{F=0}$ is assumed to be constant. The particle surface behaviours are influenced by mobile adsorption layers due to molecular rearrangement. The Hamaker constant $C_{H,sls}$ [23] includes these solid-liquid-solid interactions of continuous media. Thus $C_{H,sls}$ can be calculated due to Lifshitz theory and depends on dielectric constants and refractive indices [22, 24].

The elastic-plastic contact area coefficient κ_A represents the ratio of plastic particle contact deformation area A_{pl} to total contact deformation area $A_K = A_{pl} + A_{el}$ including a certain elastic displacement [28]

$$\kappa_A = \frac{2}{3} + \frac{1}{3}\frac{A_{pl}}{A_K} = 1 - \frac{1}{3}\sqrt[3]{\frac{h_{K,f}}{h_K}} , \tag{6}$$

with the centre approach $h_{K,f}$ for incipient yielding at point *Y* in Fig. 3, $p_{el}(r_K = 0) = p_{max} = p_f$

$$h_{K,f} = d\left(\frac{\pi p_f}{2E^*}\right)^2 , \tag{7}$$

and the averaged modulus of elasticity E^* of both particles 1and 2 (ν Poisson's ratio).

$$E^* = 2\left(\frac{1-\nu_1^2}{E_1} + \frac{1-\nu_2^2}{E_2}\right)^{-1} . \tag{8}$$

Constant mechanical bulk properties provided, the finer the particles the smaller is again the yield point $h_{K,f}$ which is shifted towards zero centre approach. Thus, an initial

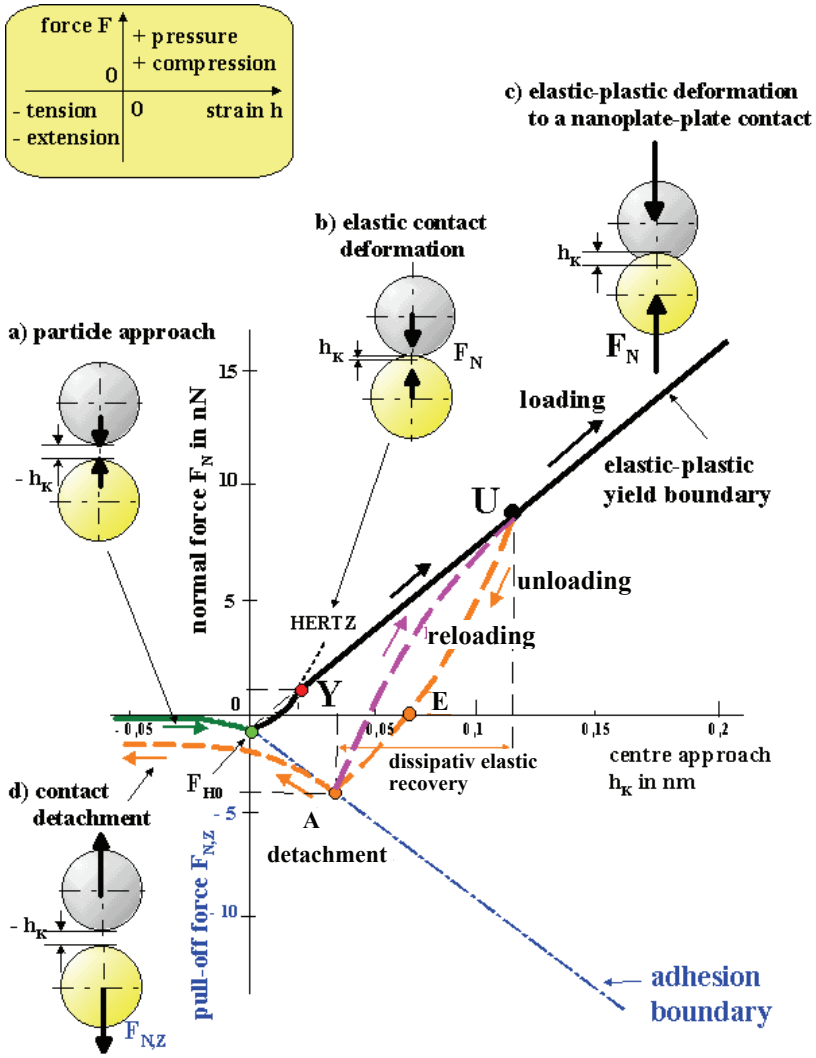

Fig. 3 Force - displacement diagram of recalculated characteristic contact deformation of very cohesive titania particles as spheres, surface diameter d_S = 200 nm, surface moisture X_W = 0,4 %. *The origin of this diagram* $h_K = 0$ *is equivalent to the characteristic adhesion separation for direct contact* $a_{F=0}$. *After loading* 0 – *Y the contact is elastically compacted with an approximated circular contact area, Fig.* 2, *b) and starts at the yield point Y at* $p_{max} = p_f$ *with plastic yielding, Fig.* 2, *c). Next, the combined elastic-plastic yield boundary of the plate-plate contact is achieved, Eq.* (3). *This displacement is expressed by annular elastic* A_{el} (*thickness* $r_{K,el}$) *and circular plastic* A_{pl} (*radius* $r_{K,pl}$) *contact area, Fig.* 2, *c). After unloading between the points U – A the contact recovers elastically according to Eq.* (9) *to a displacement* $h_{K,A}$. *The reloading curve runs from point A to U to the displacement* $h_{K,U}$, *Eq.* (10). *If one applies a certain pull-off force* $F_{N,Z} = -F_{H,A}$ *as given in Eq.* (11) *but here negative, the adhesion boundary line at failure point A is reached and the contact plates fail and detach with the increasing distance* $a = a_{F=0} + h_{K,A} - h_K$, *Fig.* 2 *panel d). This actual particle separation is considered for the calculation by a hyperbolic adhesion force curve* $F_{N,Z} = -F_{H,A} \propto a^{-3}$ *of the plate-plate model. This hysteresis behaviour could be shifted along the elastic-plastic boundary and depends on the pre-loading or, in other words, on pre-consolidation level* $F_{N,U}$. *Thus, the variation in adhesion forces* $F_{H,A}$ *between particles depend directly on this frozen irreversible deformation, the so-called contact pre-consolidation history* $F_H(F_N)$, *see next Fig.* 4

pure elastic contact deformation $A_{pl} = 0$, $\kappa_A = 2/3$, has no relevance for cohesive nanoparticles and should be excluded. But after unloading beginning at point U along curve $U - E$, Fig. 3, the contact recovers elastically in the compression mode and remains with a perfect plastic displacement $h_{K,E}$. For this pure plastic contact deformation $A_{el} = 0$ and $A_K = A_{pl}$, $\kappa_A = 1$ is obtained.

Below point E left the tension mode begins. Between $U - E - A$ the contact recovers probably elastically along a supplemented Hertzian parabolic curvature up to displacement $h_{K,A}$:

$$F_{N,unload} = \frac{2}{3} E^* \sqrt{r_{1,2} \left(h_K - h_{K,A} \right)^3} - F_{H,A} . \tag{9}$$

But along the symmetric curve $A - U$ the contact may be reloaded:

$$F_{N,reload} = -\frac{2}{3} E^* \sqrt{r_{1,2} \left(h_{K,U} - h_K \right)^3} + F_{N,U} . \tag{10}$$

If one applies a certain pull-off force $F_{N,Z} = - F_{H,A}$, here negative,

$$F_{H,A} = F_{H0} + \pi r_{1,2} p_{VdW} h_{K,A} \tag{11}$$

the adhesion (failure) boundary at point A is reached and the contact plates are failing and detaching with the increasing distance $a = a_{F=0} + h_{K,A} - h_K$. This actual particle separation can be considered for the calculation by means of a long-range hyperbolic adhesion force curve $F_{N,Z} = -F_{H,A} \propto a^{-3}$ with the plate-plate model as given in Eq. (5).

Additionally, if one considers a single elastic-plastic particle contact as a conservative mechanical system without heat dissipation, the energy absorption equals the lens-shaped area between both unloading and reloading curves $A - U$ in Fig. 3:

$$W_{diss} = \int_{h_{K,A}}^{h_{K,U}} F_{N,reload}(h_K) \; dh_K - \int_{h_{K,A}}^{h_{K,U}} F_{N,unload}(h_K) dh_K . \tag{12}$$

With Eqs. (9) and (11) for $F_{H,A}$ and (10), (3) for $F_{N,U}$, one obtains finally the specific or mass related energy absorption $W_{m,diss} = k W_{diss} / m_P$, which includes the averaged particle mass $m_P = 4/3 \pi r_{1,2}^3 \rho_s$. In addition, the resultant Eq. (3) includes a characteristic contact number in the bulk powder (coordination number $k \approx \pi/\varepsilon$ [4]):

$$W_{m,diss} = \frac{-E^*}{20 \varepsilon \rho_s} \left(\frac{h_{K,U} - h_{K,A}}{r_{1,2}} \right)^{5/2} + \frac{3 \pi p_f \left(h_{K,U} - h_{K,A} \right)}{32 r_{1,2}^2 \varepsilon \rho_s} \left[\kappa_A h_{K,U} - \kappa_p \left(h_{K,U} - h_{K,A} \right) \right] . \tag{13}$$

This specific energy of 3 to 85 $\mu J/g$ for the titania powder example mentioned was dissipated during one unloading - reloading - cycle in the bulk powder with an average pressure of only $\sigma_{M,st} = 2 \ldots 18$ kPa (or major principal stress $\sigma_1 = 4 \ldots 33$ kPa).

The slopes of elastic-plastic yield and adhesion boundaries in Fig. 3 are characteristics of irreversible particle contact stiffness or compliance. Consequently, if one eliminates the deformation h_K the linear adhesion-normal force function $F_H = f(F_N)$ in Fig. 4 is obtained [28].

$$F_H = \frac{\kappa_A}{\kappa_A - \kappa_p} F_{H0} + \frac{\kappa_p}{\kappa_A - \kappa_p} F_N = (1 + \kappa) F_{H0} + \kappa F_N . \tag{14}$$

The dimensionless elastic-plastic contact consolidation coefficient (strain characteristic) κ is given by the slope of adhesion force F_H influenced by predominant plastic contact failure.

$$\kappa = \frac{\kappa_p}{\kappa_A - \kappa_p}. \qquad (15)$$

This elastic-plastic contact consolidation coefficient κ is a measure of irreversible particle contact stiffness or softness as well. A shallow slope implies low adhesion level $F_H \approx F_{H0}$ because of stiff particle contacts, but a large slope means soft contacts, or i.e., a cohesive powder flow behaviour. This model considers, additionally, the flattening of soft particle contacts caused by the adhesion force $\kappa \cdot F_{H0}$. Thus, the total adhesion force consists of a stiff contribution F_{H0} and a contact strain influenced component $\kappa(F_{H0} + F_N)$, Fig. 4.

This Eq. (14) can be interpreted as a general linear particle contact constitutive model, i.e. linear in forces, but non-linear concerning material characteristics. The intersection of function (14) with abscissa ($F_H = 0$) in the negative extension range of consolidation force F_N is surprisingly independent of the Hamaker constant $C_{H,sls}$, Fig. 4:

$$F_{N,Z} = -\frac{\pi}{2} a_{F=0} h_r p_f \left(\frac{2}{3} + \frac{A_{pl}}{3A_K} \right) \left[1 + \frac{d/h_r}{2\left(1 + h_r / a_{F=0}\right)^2} \right] \approx -\frac{\pi}{2} a_{F=0} h_r p_f . \qquad (16)$$

Considering the model prerequisites for cohesive powders, this minimum normal (tensile) force limit $F_{N,Z}$ combines the opposite influences of a particle stiffness, micro-yield strength $p_f \approx 3\sigma_f$ or resistance against plastic deformation and particle distance distribution. The last-mentioned is characterised by roughness height h_r as well as molecular centre distance $a_{F=0}$. It corresponds to an abscissa intersection $\sigma_{1,Z}$ of the constitutive consolidation function, Eq. (28) and Fig. 7.

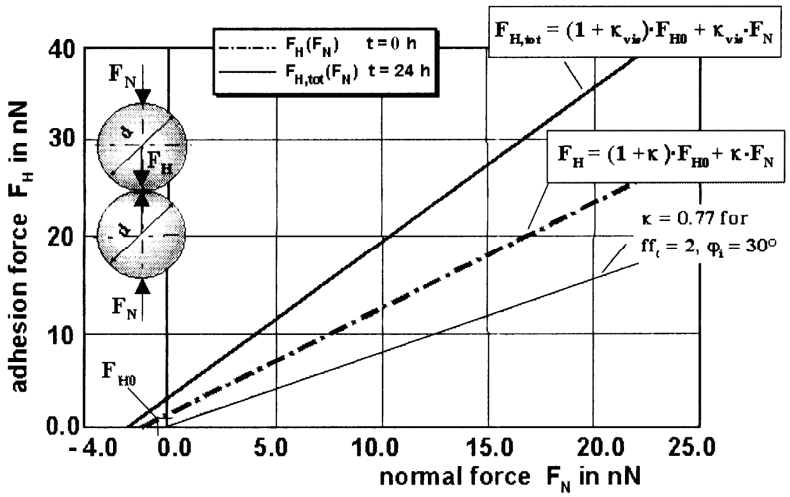

Fig. 4 Adhesion force – normal force diagram of recalculated particle contact forces of titania according to Eq. (4) using data of Fig. , surface diameter d_S = 200 nm, surface moisture X_W = 0,4 %. *This is equivalent to idealised mono-molecular adsorption layers being in equilibrium with ambient air temperature of* 20 °C *and* 50 % *humidity. The points characterise the pressure levels of the yield loci YL* 1 *to YL* 4 *according to Fig.* 7. *A characteristic line for* κ = 0,77 *of a very cohesive powder is included and shows directly the correlation between strength and force enhancement with pre-consolidation, Eq.* (31)

Cohesive Powder Flow Criteria

Using the elastic-plastic particle contact constitutive model Eq. (14) the failure conditions of particle contacts are formulated [30]. It should be noted that the stressing pre-history of a cohesive powder flow is stationary (steady-state) and delivers significantly a *cohesive* stationary yield locus in the τ-σ-diagram of Fig. 5, [28]:

$$\tau_{st} = \tan\varphi_{st}(\sigma_{st} + \sigma_0)\,. \tag{17}$$

This shear zone is characterised by a dynamic equilibrium of simultaneous contact shearing, unloading and failing, creating new contacts, loading, reloading, unloading and shearing again. The stationary yield locus is the envelope of all Mohr-circles for steady-state flow (critical state line) with a certain negative intersection of the abscissa

$$\sigma_0 = \frac{1-\varepsilon_0}{\varepsilon_0}\cdot\frac{F_{H0}}{d^2}\,. \tag{18}$$

This isostatic tensile strength σ_0 of an unconsolidated powder without any particle contact deformation is obtained from the adhesion force F_{H0}, Eq. (1), with the initial porosity of very loose packing $\varepsilon_0 = 1-\rho_{b,0}/\rho_s$, Eq. (34).

From the above formulation for cohesive steady-state flow Eq. (17), the stress-dependent effective angle of internal friction φ_e as introduced by Jenike [1], i.e., slope of *cohesionless* effective yield locus, follows in accordance with experimental experience [28]:

$$\sin\varphi_e = \sin\varphi_{st}\left(\frac{\sigma_1+\sigma_0}{\sigma_1 - \sin\varphi_{st}\cdot\sigma_0}\right) \tag{19}$$

If the major principal stress σ_1 reaches the stationary uniaxial compressive strength $\sigma_{c,st}$, the effective angle of internal friction amounts to $\varphi_e = 90°$ and for $\sigma_1 \to \infty$ follows $\varphi_e \to \varphi_{st}$. For the combination of angle of internal friction φ_i for incipient contact failure (slope of yield locus) with the stationary angle of internal friction φ_{st} following relation is used [4, 30]:

$$\tan\varphi_{st} = (1+\kappa)\tan\varphi_i \tag{20}$$

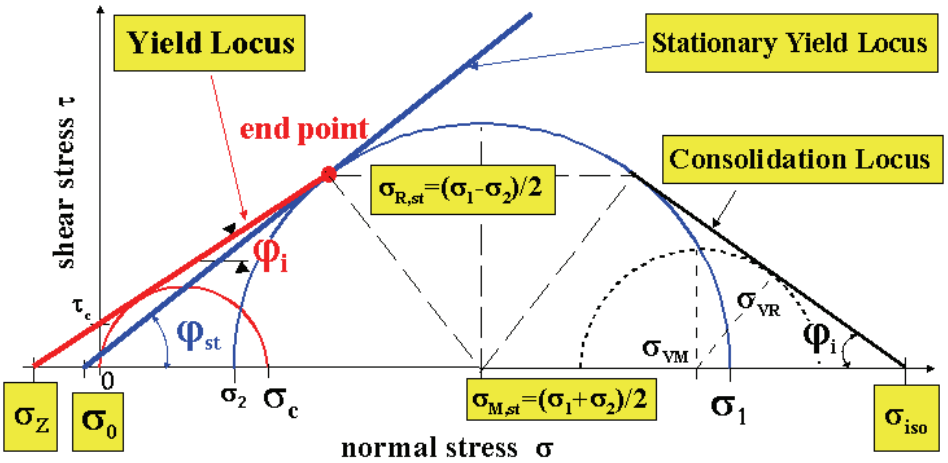

Fig. 5 Shear stress – normal stress diagram of yield characteristics of a cohesive powder. In general, the steady-state flow of a cohesive powder is cohesive. *Hence, the total normal stress consists of an external contribution* σ, *e.g. by weight of powder layers, plus* (*by absolute value*) *an internal contribution by pre-consolidation dependent adhesion* (*tensile stress* σ_Z)

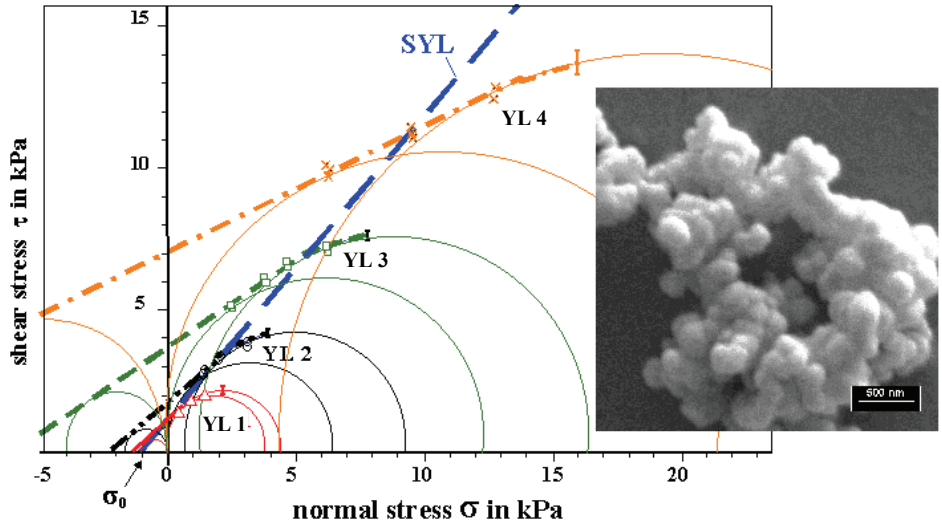

Fig. 6 Shear stress – normal stress diagram of yield loci (YL) and stationary yield locus (SYL) of titania powder, straight line regression fit ≥ 0,97, surface diameter d_S = 200 nm, solid density ρ_s = 3870 kg/m^3, shear rate v_S = 2 mm/min, surface moisture X_W = 0,4 % accurately analysed by Karl Fischer titration; angles of internal friction φ_i = 25…37°, stationary angle of internal friction φ_i = 54°, isostatic tensile strength σ_0 = 0,33 kPa

The softer the particle contacts, the larger are the differences between these friction angles and consequently, the more cohesive is the powder response.

The instantaneous yield locus describes the limit of incipient plastic powder deformation or yield. A linear yield locus, Fig. 5, is obtained from resolution of a general square function [30], is simply to use ($\sigma_{M,st}$, $\sigma_{R,st}$ centre and radius of Mohr circle for steady-state flow as parameter of powder pre-consolidation):

$$\tau = \tan\varphi_i\left(\sigma+\sigma_Z\right) = \tan\varphi_i\left(\sigma+\frac{\sigma_{R,st}}{\sin\varphi_i}-\sigma_{M,st}\right). \qquad (21)$$

It is worth to note here that only the isostatic tensile strength σ_Z for incipient yield depends directly on the consolidation pre-history and is given by:

$$\sigma_Z = \frac{\sigma_{R,st}}{\sin\varphi_i}-\sigma_{M,st} = \left(\frac{\sin\varphi_{st}}{\sin\varphi_i}-1\right)\sigma_{M,st}+\frac{\sin\varphi_{st}}{\sin\varphi_i}\sigma_0\,. \qquad (22)$$

The smaller a radius stress for pre-consolidation $\sigma_{VR} < \sigma_{R,st}$, the larger is the centre stress $\sigma_{VM} > \sigma_{M,st}$ right of largest Mohr circle for steady-state flow in Fig. 5, and the smaller may be the powder tensile strength σ_Z. The so-called consolidation locus lies at the right hand side and represents the envelope of all Mohr circles for consolidation stresses with plastic powder failure, Fig. 5, i.e. the radius σ_{VR} and centre σ_{VM} stresses. Provided that the particle contact failure is equivalent to that between incipient powder flow and consolidation, one can write for a linear consolidation locus with negative slope -sinφ_i which is symmetrically with the linear yield locus, Eq. (26):

$$\sigma_{VR} = \sin\varphi_i\left(-\sigma_{VM}+\sigma_{iso}\right). \qquad (23)$$

Due to this symmetry between yield and consolidation locus, one can directly estimate the isostatic powder compression $\sigma_1 = \sigma_2 = \sigma_{VM} = \sigma_{iso}$ from Fig. 5 for the radius stress $\sigma_{VR} = 0$:

$$\sigma_{iso} = 2\sigma_{M,st} + \sigma_Z = \frac{\sigma_{R,st}}{\sin\varphi_i} + \sigma_{M,st} = \left(\frac{\sin\varphi_{st}}{\sin\varphi_i} + 1\right)\sigma_{M,st} + \frac{\sin\varphi_{st}}{\sin\varphi_i}\sigma_0 . \qquad (24)$$

Generally, when we use these radius σ_R and centre stresses σ_M, the essential flow parameters are compiled as one set of linear constitutive equations, i.e. for instantaneous consolidation, the consolidation locus (CL),

$$\sigma_R = \sin\varphi_i\left(-\sigma_M + \sigma_{M,st}\right) + \sigma_{R,st} , \qquad (25)$$

for incipient yield, the yield locus (YL),

$$\sigma_R = \sin\varphi_i\left(\sigma_M - \sigma_{M,st}\right) + \sigma_{R,st} \qquad (26)$$

and for steady-state flow, the stationary yield locus (SYL):

$$\sigma_{R,st} = \sin\varphi_{st}\left(\sigma_{M,st} + \sigma_0\right) \qquad (27)$$

These yield functions are completely described only with three material parameters plus the characteristic pre-consolidation stress $\sigma_{M,st}$ or average pressure influence, see Tomas [30]:

(1) φ_i – incipient particle friction of failing contacts, i.e. Coulomb friction;

(2) φ_{st} – steady-state particle friction of failing contacts, increasing adhesion by means of flattening of contact expressed with the contact consolidation coefficient κ, or by friction angles $\left(\sin\varphi_{st} - \sin\varphi_i\right)$ as shown in the next Eqs. (28) and (29). The softer the particle contacts, the larger are the difference between these friction angles the more cohesive is the powder;

(3) σ_0 – extrapolated isostatic tensile strength of unconsolidated particle contacts without any contact deformation, equals a characteristic cohesion force in an unconsolidated powder;

(4) $\sigma_{M,st}$ – previous consolidation influence of an additional normal force at particle contact, characteristic centre stress of Mohr circle of pre-consolidation state directly related to powder bulk density. This average pressure influences the increasing isostatic tensile strength of yield loci via the cohesive steady-state flow as the stress history of the powder.

These physically based flow parameters are necessary to derive the uniaxial compressive strength σ_c which is simply found from the linear yield locus, Eq. (26) and Fig. 5, for $\sigma_c = 2\cdot\sigma_R$ ($\sigma_2 = 0$ and $\sigma_R = \sigma_M$) as a linear function of the major principal stress σ_1, Fig. 7, [28]:

$$\sigma_c = \frac{2\left(\sin\varphi_{st} - \sin\varphi_i\right)}{\left(1+\sin\varphi_{st}\right)\left(1-\sin\varphi_i\right)}\sigma_1 + \frac{2\sin\varphi_{st}\left(1+\sin\varphi_i\right)}{\left(1+\sin\varphi_{st}\right)\left(1-\sin\varphi_i\right)}\sigma_0 . \qquad (28)$$

Equivalent to this linear function of the major principal stress σ_1 and using again Eq. (26), the absolute value of the uniaxial tensile strength $\sigma_{Z,1}$ is also found for $\sigma_{Z,1} = -\sigma_R$ ($\sigma_1 = 0$ and $\sigma_R = -\sigma_M$):

$$\sigma_{Z,1} = \frac{2\cdot\left(\sin\varphi_{st} - \sin\varphi_i\right)}{\left(1+\sin\varphi_{st}\right)\left(1+\sin\varphi_i\right)}\sigma_1 + \frac{2\sin\varphi_{st}}{1+\sin\varphi_{st}}\sigma_0 . \qquad (29)$$

Both flow parameters σ_c and $\sigma_{Z,1}$ depend on the pre-consolidation level of the shear zone which is expressed by the applied consolidation stress for steady-state flow σ_1. A considerable time consolidation under this major principal stress σ_1 after one day storage at rest is also shown in Fig. 7. Equivalent linear functions are also used to describe these time consolidation effects [30].

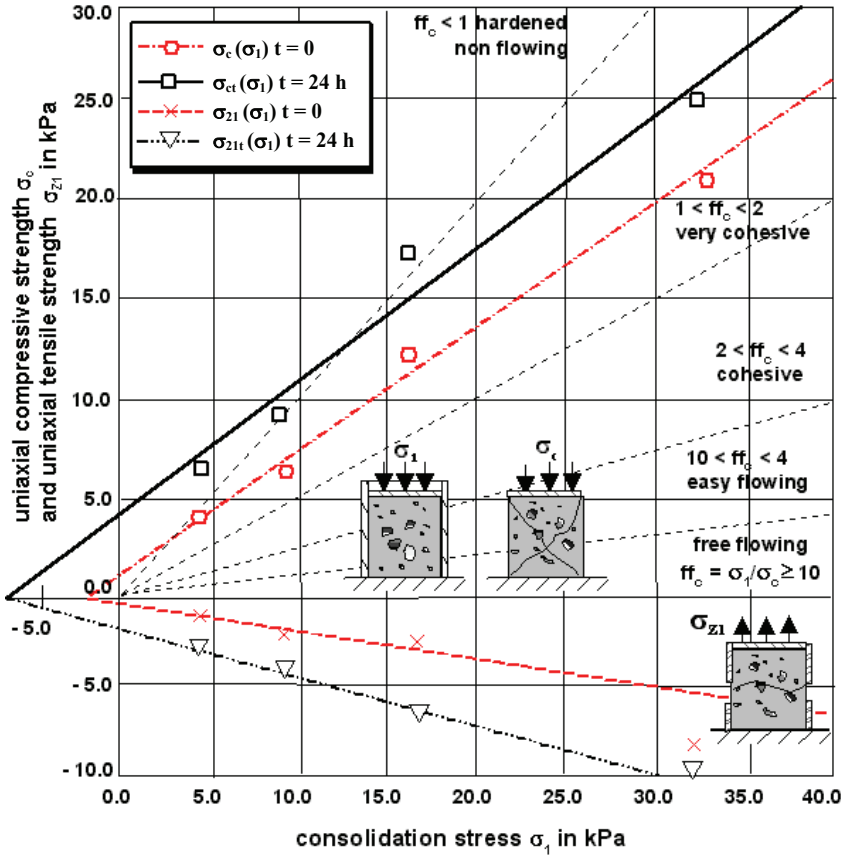

Fig. 7 Powder strength - consolidation stress diagram of constitutive consolidation function of titania, straight line regression fit = 0,99, d_S = 200 nm, X_W = 0,4 %

Powder Flowability and Compressibility

In order to assess the flow behaviour of a powder, Eq. (28) shows that the flow function due to Jenike [1] $ff_c = \sigma_1 / \sigma_c$ is not constant and depends on the pre-consolidation level σ_1. Approximately, one can write for a small intercept with the ordinate $\sigma_{c,0}$, Fig. 7, the stationary angle of internal friction is equivalent to the effective angle $\varphi_{st} \approx \varphi_e$ and Jenike's [1] formula is obtained:

$$ff_c \approx \frac{(1+\sin\varphi_e)(1-\sin\varphi_i)}{2(\sin\varphi_e - \sin\varphi_i)}. \qquad (30)$$

Thus, the semi-empirical classification by means of the flow function introduced by Jenike [1] is adopted here with considerations for certain particle behaviour, Table 1.

Obviously, the flow behaviour is mainly influenced by the difference between the friction angles, Eq.(30), as a measure for the adhesion force slope κ in the general linear particle contact constitutive model, Eq. (15). Thus one can directly correlate κ with flow function ff_c [30]:

$$\kappa = \frac{1+(2ff_c-1)\sin\varphi_i}{\tan\varphi_i\,(2ff_c-1+\sin\varphi_i)} \sqrt{\frac{1}{1-\left(\frac{1+(2ff_c-1)\sin\varphi_i}{2ff_c-1+\sin\varphi_i}\right)^2}} - 1. \qquad (31)$$

Table 1

Flowability assessment and elastic-plastic contact consolidation coefficient $\kappa(\varphi_i = 30°)$

flow function ff_c	κ-values	φ_{st} in deg	evaluation	Examples
100…10	0,01006…0,107	30,3…33	free flowing	dry fine sand
4…10	0,107…0,3	33…37	easy flowing	moist fine sand
2…4	0,3…0,77	37…46	cohesive	dry powder
1…2	0,77…∞	46…90	very cohesive	moist powder
< 1	∞	–	non flowing	moist powder

A characteristic value $\kappa = 0{,}77$ for $\varphi_i = 30°$ of a very cohesive powder is included in the adhesion force diagram, Fig. 4, and shows directly the correlation between strength and force increasing with pre-consolidation, Table 1. Due to the consolidation function, a small slope designates a free flowing particulate solid with very low adhesion level because of stiff particle contacts but a large slope implies a very cohesive powder flow behaviour because of soft particle contacts, Fig. 7.

Obviously, the finer the particles the "softer" are the contacts and the more cohesive is the powder [27, 28]. Köhler [31] has experimentally confirmed this thesis for alumina powders (α-Al_2O_3) down to the sub-micron range ($\sigma_{c,0} \approx$ const = 2 kPa, d_{50} median particle size in μm):

$$ff_c \approx 2{,}2 d_{50}^{0{,}62}. \tag{32}$$

A survey of uniaxial compression equations was given by Kawakita [32]. Thus in terms of a moderate cohesive powder compression, to draw an analogy to the adiabatic gas law $pV^{\kappa_{ad}} = \text{const}$, a differential equation for isentropic compressibility of a powder $dS = 0$, i.e. remaining stochastic homogeneous (random) packing without a regular order in the continuum, is derived, beginning with:

$$\frac{d\rho_b}{\rho_b} = n\frac{dp}{p} = n\frac{d\sigma_{M,st}}{\sigma_{M,st} + \sigma_0}. \tag{33}$$

The total pressure including particle interaction $p = \sigma_{M,st} + \sigma_0$ should be equivalent to a pressure term with molecular interaction $\left(p + a_{VdW}/V_m^2\right)\left(V_m - b\right) = RT$ in van der Waals equation of state to be valid near gas condensation point. A "condensed" loose powder packing is obtained $\rho_b = \rho_{b,0}$, if only particles are interacting without an external consolidation stress $\sigma_{M,st} = 0$, e.g. particle weight compensation by a fluid drag, and Eq. (33) is solved:

$$\frac{\rho_b}{\rho_{b,0}} = \left(\frac{\sigma_0 + \sigma_{M,st}}{\sigma_0}\right)^n. \tag{34}$$

Therefore, this physically based compressibility index $n \equiv 1/\kappa_{ad}$ lies between $n = 0$, i.e. incompressible stiff bulk material and $n = 1$, i.e. ideal gas compressibility. Considering the predominant plastic particle contact deformation in the stochastic homogeneous packing of a cohesive powder, following values of compressibility index are recommended in Table 2.

Table 2

Compressibility index of powders, semi-empirical estimation for σ_1 = 1…100 kPa

index *n*	evaluation	examples	flowability
0…0,01	incompressible	gravel	free flowing
0,01…0,05	low compressibility	fine sand	
0,05…0,1	compressible	dry powder	cohesive
0,1…1	very compressible	moist powder	very cohesive

Generally, the influence of micro-properties as particle contact stiffness on the macro-behaviour as powder flow properties, i.e. cohesion, flowability and compressibility, can be directly shown in Fig. 8.

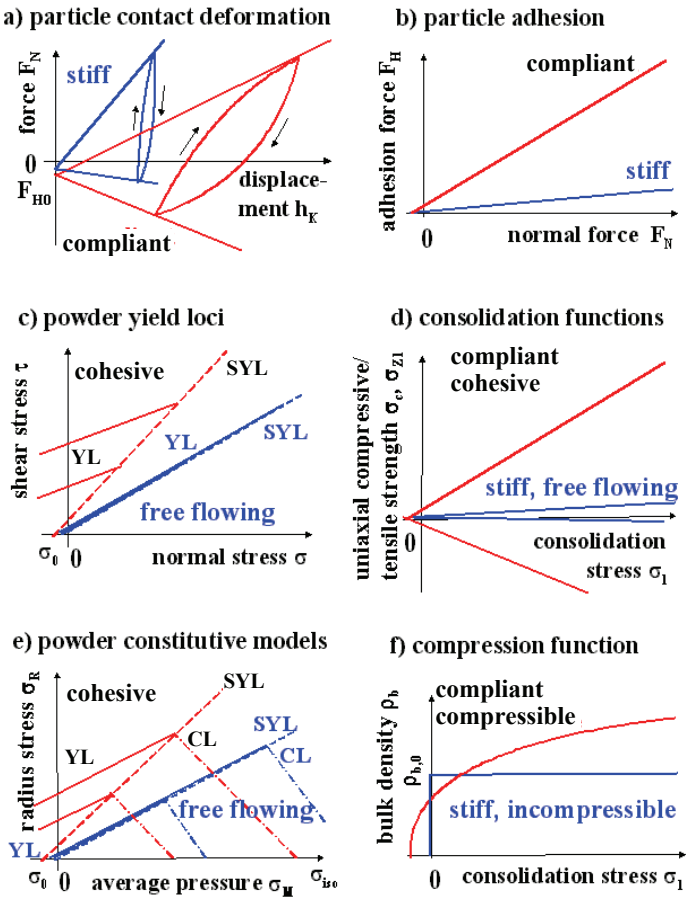

Fig. 8 Characteristic constitutive functions of stiff and compliant particle contact behaviours, free flowing and cohesive powder behaviours, and finally, stiff incompressible and soft compressible powders [40]. *Increasing contact compliance determine decreasing slope of the elastic-plastic yield boundary (limit) and increasing inclination of the adhesion boundary or limit. As the result, the slope of the normal force-adhesion force function increases. Next, the difference between the stationary angle and angle of internal friction of the powder becomes larger. Consequently, the slope of the powder consolidation function increases and the powder is more compressible*

Conclusions

A complete set of physically based equations for steady-state flow, incipient powder consolidation and yielding, compressibility and flowability has been shown. Using this, the yield surfaces due to theory of plasticity may be described with very simple linear expressions:

$$\Phi_{YL,SYL,CL} = 0 = \begin{cases} \sigma_R - \sin\varphi_i\left(\sigma_M - \sigma_{M,st}\right) - \sigma_{R,st} & \text{yield locus (YL)} \\ \sigma_{R,st} - \sin\varphi_{st}\left(\sigma_{M,st} + \sigma_0\right) & \text{stationary yield locus (SYL)} \\ \sigma_R - \sin\varphi_i\left(-\sigma_M + \sigma_{M,st}\right) - \sigma_{R,st} & \text{consolidation locus (CL)} \end{cases} \quad (35)$$

The consolidation and yield loci and the stationary yield locus are completely described only with three material parameters, i.e., angle of internal friction φ_i, stationary angle of internal friction φ_{st}, isostatic tensile strength of an unconsolidated powder σ_0 plus the characteristic pre-consolidation (average pressure) influence $\sigma_{M,st}$. The compressibility index n as an additional constitutive bulk powder parameter was introduced and the classification $0 \le n < 1$ recommended. A direct correlation between flow function ff_c and elastic-plastic contact consolidation coefficient κ was derived.

This approach has been used to evaluate the powder flow properties concerning various particle size distributions (nanoparticles to granules), moisture contents (dry, moist and wet) and material properties (minerals, chemicals, pigments, waste, plastics, food etc.), which have been tested and evaluated for more than the last 20 years [27]. Thus, these models are directly applied to evaluate the test data of a new oscillating shear cell [33, 34,35] and a press-shear-cell in the high-level pressure range from 50 to 2000 kPa for liquid saturated, compressible filter cakes [36, 37,38] and for dry powders [39]. Additionally, the force – displacement behaviour during stressing and the breakage probability are useful constitutive functions to describe the mechanics of agglomerates to assess the physical product quality [43]. These contact models are also needed to simulate the shear dynamics of cohesive powders using the discrete element method (DEM) and to calibrate these simulations by shear cell measurements [44].

The influence of particle surface properties, e.g. as contact stiffness, on the powder flow properties can be directly interpreted, Fig. 8, and practically used to design particulate products in process industries [42, 45].

Acknowledgements

The author would like to acknowledge his co-workers Dr. S. Aman, Dr. T. Gröger, Dr. W. Hintz, Dr. Th. Kollmann and Dr. B. Reichmann for providing relevant information and theoretical tips. The advices from H.-J. Butt [46] *and S. Luding* [47] *with respect to the fundamentals of particle and powder mechanics were especially appreciated during the collaboration of the project "shear dynamics of cohesive, fine-disperse particle systems" of the joint research program "Behaviour of Granular Media" of German Research Association (DFG).*

References

1. Jenike A. W. (1964) Storage and flow of solids, Engng. Exp. Stat. Bull. No. 123, Univ. Utah.

2. Schwedes J. and Wilms H. (1988) Fließeigenschaften von Schüttgütern, pp 39-58, in: Martens P, Silo – Handbuch, Ernst & Sohn Berlin.

3. Schwedes J. and Schulze D. (2003) Lagern von Schüttgütern, pp 1137-1253, in Schubert H (Ed.) Handbuch der Mechanischen Verfahrenstechnik, Whiley-VCH, Weinheim.

4. Molerus O. (1975) Theory of yield of cohesive powders, Powder Technology 12 pp 259-275.

5. Molerus O. (1978) Effect of interparticle cohesive forces on the flow behaviour of powders, Powder Technology 20 pp 161-175.

6. Hertz H. (1882) Über die Berührung fester elastischer Körper, J. reine u. angew. Math. 92 pp 156-171.

7. Huber M. T. (1904) Zur Theorie der Berührung fester elastischer Körper, Annal. Physik 14 pp 153-163.

8. Mindlin R. D. and Deresiewicz H. (1953) Elastic spheres in contact under varying oblique forces, J. Appl. Mech., Trans. ASME 20 pp 327-344.

9. Dahneke B. (1972) The influence of flattening on the adhesion of particles, J. Colloid and Interface Sci. 40 pp 1-13.

10. Derjaguin B. V., Muller V. M. and Toporov U. P. (1975) Effect of contact deformations on the adhesion of particles, J. Colloid and Interface Sci. 53 pp 314-326.

11. Johnson K. L. (1985) Contact Mechanics, Cambridge University Press.

12. Thornton C. and Yin K. K. (1991) Impact of elastic spheres with and without adhesion, Powder Technology 65 pp 153-166.

13. Sadd M. H., Tai Q. and Shukla A. (1993) Contact law effects on wave propagation in particulate materials using distinct element modeling, Int. J. Non-Linear Mechanics 28 pp 251-265.

14. Derjaguin B. V. (1934) Untersuchung über die Reibung und Adhäsion, IV – Theorie des Anhaftens kleiner Teilchen, Kolloid Zeitschr. 69 pp 155-164.

15. Krupp H. (1967) Particle Adhesion – Theorie and Experiment, Advanced Colloid Interface Sci. 1 pp 111-239.

16. Schubert H., Sommer K. and Rumpf H. (1976) Plastisches Verformen des Kontaktbereiches bei der Partikelhaftung, Chem.-Ing.-Tech. 48 pp 716 .

17. Maugis D. and Pollock H. M. (1984) Surface forces, deformation and adherence at metal microcontacts, Acta Metall. 32 pp 1323-1334.

18. Walton O. R. and Braun R. L. (1986) Viscosity, granular temperature and stress calculations for shearing assemblies of inelastic, frictional discs, J. Rheol. 30 pp 949-980.

19. Thornton C. and Ning Z. (1998) A theoretical model for the stick/bounce behaviour of adhesive, elastic-plastic spheres, Powder Technology 99 pp 154-162.

20. Wei Hsuin Yang (1966) The contact problem for viscoelastic bodies, J. Appl. Mech., Trans. ASME 33 pp 395-401.

21. Rumpf H., Sommer K. and Steier K. (1976) Mechanismen der Haftkraftverstärkung bei der Partikelhaftung durch plastisches Verformen, Sintern und viskoelastisches Fließen, Chem.-Ing.-Tech. 48 pp 300-307.

22. Israelachvili J. N. (1992) Intermolecular and surface forces, Academic Press London.

23. Hamaker H. C. (1937) The London – van der Waals attraction between spherical particles, Physica 4 pp 1058-1072.

24. Lifshitz E. M. (1956) The theory of molecular attractive forces between solids Soviet. Phys. JETP 2 pp 73-83.

25. Schubert H. (1982) Kapillarität in porösen Feststoffsystemen, Springer Verlag Berlin.

26. Rabinovich Y. I., Adler J. J., Ata A, Moudgil B M and Singh R K (2000) J. Colloid Interface Sci. 232 pp 10-16.

27. Tomas J. (1991) Modellierung des Fließverhaltens von Schüttgütern auf der Grundlage der Wechselwirkungskräfte zwischen den Partikeln und Anwendung bei der Auslegung von Bunkeranlagen, Habilitation, Bergakademie Freiberg.

28. Tomas J. (2000) Particle Adhesion Fundamentals and Bulk Powder Consolidation, KONA – Powder and Particle 18 pp 157-169.

29. Tomas J. (2001) Assessment of mechanical properties of cohesive particulate solids – part 1: particle contact constitutive model, Particulate Sci. & Technology 19 pp 95-110.

30. Tomas J. (2001) Assessment of mechanical properties of cohesive particulate solids – part 2: powder flow criteria, Particulate Sci. & Technology 19 pp 111-129.

31. Köhler Th. and Schubert H. (1990) Influence of particle size distribution on the flow behaviour of fine powders, Part. Part. Syst. Charact. 8 pp 101-104.

32. Kawakita K. and Lüdde K-H. (1970/17) Some considerations on powder compression equations, Powder Technology 4 pp 61-68.

33. Kollmann Th. and Tomas J. (2001) The Influence of Vibrations on Flow Properties of Cohesive Powders, pp 417-427, Int. Conf. Bulk Materials Storage, Handling and Transportation, Vol 1, Newcastle.

34. Kollmann Th. and Tomas J. (2002) Effect of Applied Vibrations on Silo Hopper Design, Particulate Sci. & Technology 20 pp 15-31.

35. Haack A. and J. Tomas, Untersuchungen zum Dämpfungsverhalten hochdisperser kohäsiver Pulver, Chem.- Ing.- Technik 75 (2003), submitted.

36. Reichmann B. and Tomas J. (2001) Expression behaviour of fine particle suspensions and the consolidated cake strength, Powder Technology 121 pp 182-189.

37. Tomas J. and Reichmann B. (2001) Compression, permeation and flow behaviour of wet nanoparticle cakes, in-situ tested with a press-shear-cell, Filtech Europa, Vol 1, pp 47-55, Düsseldorf.

38. Mladenchev Th. and J. Tomas, Flow properties of compressed fine filtercakes, Intern. Conf. Filtech Europa 2003, Düsseldorf 2003.

39. Grossmann L., Tomas J. and Czöke B., Compressibility and flow properties of a cohesive limestone powder in a medium pressure range, in Kalman, H. and Gyenis, J., The 4th Conference for Conveying and Handling of Particulate Solids, 4.20-4.25, Budapest 2003.

40. Tomas J. (2002) Zur Mechanik trockener kohäsiver Schüttgüter, Schüttgut 8 pp 522-537 (2002).

41. Tomas J. (2003) Mechanics of Nanoparticle Adhesion – a Continuum Approach, in K.L. Mittal: Proceedings of the 8th Intern. Symp. on Particles on Surfaces: Detection, Adhesion and Removal, Providence 2002, (in print).

42. Tomas J. (2003) Zur Produktgestaltung kohäsiver Pulver – mechanische Eigenschaften, Kompressions- und Fließverhalten, Chem.- Ing.- Technik 75 pp 651 – 661.

43. Antoniuk S. and Tomas J. (2003) Mechanische Bruchprozesse in Agglomeraten bei der Druckbeanspruchung, paper, Maschinenbau und Technik des 21. Jahrh., Sevastopol.

44. Tykhoniuk R., Luding S. and Tomas J. (2003) Simulation der Scherdynamik kohäsiver Pulver, Chem.- Ing.- Technik 75 submitted.

45. Tomas J. (1983) Untersuchungen zum Fließverhalten von feuchten und leichtlöslichen Schüttgütern, Freiberger Forschungshefte A 677 pp 1 – 133.

46. Ecke S. and Butt H-J. (2001) friction between individual microcontacts, J. Colloid Interface Sci. 244 pp 432-435.

47. Luding S. and Herrmann H. J. (2001) Micro - macro transition for cohesive granular media, pp 121-134, in Diebels S: Zur Beschreibung komplexen Materialverhaltens, Institut für Mechanik, Stuttgart.

Адгезия наночастиц и текучесть когезионных нанопорошков

Ю. Томас

Кафедра «Механические процессы и аппараты»
Университет Отто-фон-Герике, Магдебург, Германия

Ключевые слова и фразы: адгезионные силы; когезия; конститутивная модель; механика порошков; механика сыпучих сред; сжимаемость порошков; силы Ван-дер-Ваальса; текучесть порошков; функция свойств; TiO_2-нанопорошок.

Аннотация: Описаны основы свойств упрочнения и текучести когезионных порошков на базе объединения механики частиц и механики непрерывной среды. С помощью модели «жесткая частица с мягкими контактами» показано влияние упруго-пластичного отталкивания при контакте частиц. На этих физических основах представлены стационарная линия текучести, индивидуальные линии текучести, линии упрочнения, функция текучести сильно когезионного TiO_2-нанопорошка (гидравлический диаметр d_s = 200 нм). Модели используются для оценки результатов сдвиговых испытаний. Эти функции свойств используются также для компьютерных расчетов технологических аппаратов на надежное истечение порошка.

Nanopartikelhaftung und Fliesseigenschaften kohäsiver Nanopulver

Zusammenfassung: Die Grundlagen des Verfestigungsverhaltens und des Fließverhaltens kohäsiver Pulver werden erläutert, in dem die Partikelmechanik und die Kontinuumsmechanik sinnvoll miteinander verknüpft werden. Mittels des Modells „steife Partikel mit weichen Kontakten“ wird der Einfluß der elastisch-plastischen Abstoßung im Partikelkontakt gezeigt. Auf dieser physikalischen Grundlage werden der stationäre Fließort, die Momentanfliessorte, die Verfestigungsorte, die Fließfunktion, die Verfestigungsfunktion und die Kompressionsfunktion anhand der Fließeigenschaften eines sehr kohäsiven TiO_2-Nanopulvers (Sauterdurchmesser d_s = 200 nm) demonstriert. Die Modelle dienen der Bewertung der Ergebnisse von Scherversuchen. Diese Eigenschaftsfunktionen werden wiederum gebraucht, um verfahrenstechnische Apparate fließgerecht und computergestützt auszulegen.

Adhésion des nanoparticules et fluidité des nanopoudres cohésives

Résumé: Sont décrites les bases des propriétés de la consolidation et de la fluidité des poudres cohésives à la base de la réunion de la mécanique des particules et celle du milieu continu. A l’aide du modèle «particule dure avec des contacts souples» on a montré l'influence de la répulsion flexible et plastique lors du contact des particules. Sur ces bases physiques sont proposées la ligne stationnaire de la fluidité, les lignes individuelles de la fluidité, les lignes du renforcement, la fonction de la fluidité de la nanopoudre TiO_2 très cohésive (le diamètre hydraulique d_s = 200 nm). Les modèles sont employés pour l’évaluation des résultats des essais de décalage. Ces fonctions sont utilisées de nouveau pour le calcul des appareils technologiques sur l’écoulement sûr de la poudre à l’aide de l’ordinateur.